

See discussions, stats, and author profiles for this publication at: <https://www.researchgate.net/publication/231701842>

Phase Selection Pathways in Ultrathin Film Crystallization of a Low Molecular Weight Poly(ethylene oxide) Fraction on Mica Surfaces

ARTICLE in MACROMOLECULES · OCTOBER 2011

Impact Factor: 5.8 · DOI: 10.1021/ma201885g

CITATIONS

4

READS

18

4 AUTHORS, INCLUDING:



Yi-Xin Liu

Fudan University

11 PUBLICATIONS 180 CITATIONS

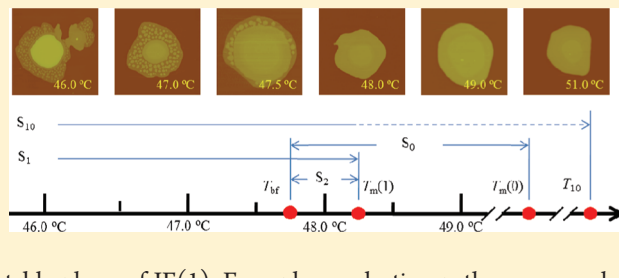
SEE PROFILE

Phase Selection Pathways in Ultrathin Film Crystallization of a Low Molecular Weight Poly(ethylene oxide) Fraction on Mica Surfaces

Yi-Xin Liu,[†] Lu-Wei Zhong, Shi-Zhao Su, and Er-Qiang Chen*

Beijing National Laboratory for Molecular Sciences, Department of Polymer Science and Engineering and Key Laboratory of Polymer Chemistry and Physics of Ministry of Education, College of Chemistry, Peking University, Beijing 100871, China

ABSTRACT: Utilizing *in situ* atomic force microscopy, we monitored the phase selection pathways of ultrathin film crystallization of a low molecular weight poly(ethylene oxide) fraction with two hydroxyl end groups and a number-average molecular weight of 3000 g/mol (HPEO3k) on mica surfaces. The sample forms integral folded chain (IF) monolayer crystals. From a thermodynamic point of view, in the vicinity of the melting temperature [$T_m(1)$] of the once-folded chain crystal [IF(1)], the system studied provides a three-phase model composed of the melt phase, the stable phase of extended chain crystals [IF(0)], and the metastable phase of IF(1). Four phase selection pathways, namely, melt \rightarrow IF(0) (S_0), melt \rightarrow IF(1) (S_1), IF(1) \rightarrow IF(0) (S_{10}), and a composite pathway built of the latter two (S_2) have been revealed experimentally. The first selected pathway at crystallization temperatures near $T_m(1)$ depends on the supercooling, in agreement with the predication of Gránásy-Oxtoby theory. Below a bifurcation point located slightly lower than $T_m(1)$, the pathway selection of isothermal crystallization is also time dependent, wherein a coexistence of S_1 , S_{10} , and S_0 at the late stage of crystallization is observed. This phenomenon is beyond expectation and may be related to the crystal growth mechanism switching from nucleation-limited to diffusion-limited.



INTRODUCTION

Understanding how long chain molecules crystallize remains one of the most challenging fundamental problems in polymer physics.^{1–4} The biggest difference between crystallization of small molecules and polymers is that the later seldom reaches the ultimate equilibrium and is usually trapped in metastable states characterized by the existence of chain folding in the resulting semicrystalline structure. Folded-chain crystals usually take the form of lamellae with their thicknesses much smaller than the lateral size and chain contour length. They can further organize into a hierarchy of ordered structures which in turn controls the physical properties of the polymeric materials. Much effort has been devoted to understanding the molecular mechanism of growing such particular forms of semicrystalline polymers since the discovery of platelet single crystals. The major theory of polymer crystallization, formulated by Lauritzen and Hoffman (LH), restricts to the growth stage of forming lamellar crystals. In this theory, the actual crystal growth rate results from the competition between the thermodynamic driving force, which is related to the supercooling, and a free energy barrier arisen from attaching a set of segments (stem) onto the growing surface. Consequently, the thickness of the growing lamella at certain supercoolings is chosen to maximize this growth rate. Although LH theory has been applied to fit experimental results successfully in many cases, it contains many short-comings. One typical example is the crystallization of low molecular weight (LMW) polymers in the vicinity of the temperature where polymer chains start to fold.

LMW polymers with nearly monodispersed molecular weight (MW) distribution and monodispersed oligomers, such as ultralong alkanes, are ideal model systems for studying the crystallization of polymers.^{1,2} The chemical composition and geometry of these kinds of molecules are simple yet still sufficient to maintain the main features of polymer crystallization. One remarkable feature of LMW polymers is that they usually form integral folded chain (IF) crystals whose thicknesses correspond to the integral fractions of the chain contour length. Hereafter, the IF crystal with n folds per chain is denoted as an IF(n) crystal. The onset of chain folding in short chains was argued to be successfully reproduced by a modified LH theory.⁵ However, as to the detail of this transition from extended chain form [IF(0)] to once-folded chain form [IF(1)], an anomalous rate minimum was observed near or at the transition point in crystallization of ultralong alkanes both from melt and from solution by Ungar and co-workers.^{6–9} The authors concluded that the surface nucleation theory was incapable of explaining this growth rate minimum.⁹ Rather, it can be best explained by treating it as an extreme case of the pinning effect in the entropic barrier model proposed by Gilmer and Sadler (GS),^{10–12} where the growth of IF(0) crystals was effectively retarded by first nucleation of wrong-configured folded chain stems on the growth front. This phenomenon is termed “self-poisoning”.⁹ An even earlier

Received: August 18, 2011

Revised: October 10, 2011

Published: October 28, 2011

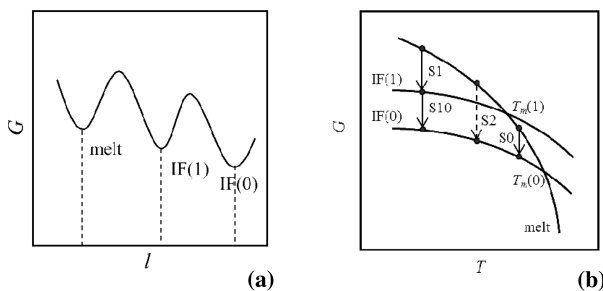


Figure 1. Schematic illustration of profiles of free energy (G) with respect to (a) crystal thickness (l) and (b) temperature (T) for LMW polymers.

observation on linear growth rate of LMW poly(ethylene oxide) (PEO) crystals reported by Kovacs et al. has shown an abrupt change of the gradient of growth rate curve versus supercooling,¹³ though the rate minimum was not observed. More recently, an actual minimum has also been realized in a LMW PEO fraction capped by methoxyl end groups.¹⁴

However, all above observations mainly focused on the growth rate as a function of supercooling, while the question of how IF(0) and IF(1) crystals grow under various supercoolings has not been demonstrated explicitly. It is now well established that IF($n > 0$) crystals are nonequilibrium structures trapped in metastable states. Especially, for IF(n) crystals of LMW polymers, they can be considered as well-defined “phases” due to the large difference in thickness leading to a large energy barrier between them. For instance, the melt, IF(0) crystal, and IF(1) crystal may be treated as a three-phase system which is similar to the conventional crystallization system composed of one liquid phase and two different crystalline phases as schematically shown in Figure 1a. It is well-known that the phase behavior in such a three-phase system containing a metastable phase is much more complicated than two-phase system. According to the classical nucleation theory (CNT), four phase selection pathways are possible in such a system: unstable phase \rightarrow stable phase, unstable phase \rightarrow metastable phase, metastable phase \rightarrow stable phase, and a composite pathway built of the latter two. The occurrence of which pathway depends on the supercooling as well as other kinetic factors. In this context, we may also expect that various kinds of phase selection pathways will be identified when LMW polymers are quenched to certain supercoolings. It can be straightforward to figure out that the four transition pathways can be: melt \rightarrow IF(0) crystals, melt \rightarrow IF(1) crystals, IF(1) crystals \rightarrow IF(0) crystals, and the composite pathway built of the latter two, which are denoted by S_0 , S_1 , S_{10} , and S_2 , respectively, in this paper. Figure 1b illustrates these phase selection pathways in a free energy \sim temperature ($G-T$) diagram. Of particular interest is how the polymer chains select their pathway to form crystalline lamellae with different thickness in the vicinity of $T_m(1)$. While S_0 shall be the only choice when the crystallization temperature (T_c) ranges from the melting temperature of IF(0) [$T_m(0)$] to the melting temperature of IF(1) [$T_m(1)$], all four pathways may compete with each other at T_c below $T_m(1)$ as shown in the $G-T$ diagram. Note that this assertion is thermodynamic in nature, which is essentially different from classical polymer crystallization theories such as LH theory and GS theory.

To elucidate the validity of the above assumption, we report a systematic study of crystallization of a LMW poly(ethylene oxide) (PEO) fraction in ultrathin films on the mica surface

under various supercoolings. Usually, a thin layer of LMW PEO will form a pseudodewetted melt structure on hydrophilic substrates at temperatures above T_m , wherein nonadsorbed PEO molecules form droplets sitting on the top of a ~ 5 nm thick wetting monolayer. This pseudodewetted melt structure is presumably due to autophobic dewetting.^{15–18} The IF(n) crystals with a constant lamellar thickness and sharp interfaces can be unambiguously distinguished from the melt by atomic force microscopy (AFM). We thus utilized *in situ* AFM to monitor the crystal growth process and the morphological evolution. The four phase selection pathways of S_0 , S_1 , S_{10} and S_2 were indeed captured at proper supercoolings, in good agreement with the prediction of a modified nucleation theory by Gránásy and Oxtoby which deals with the crystallization of a three-phase system.¹⁹ We also observed that at temperatures below a bifurcation point slightly lower than $T_m(1)$, the S_{10} process takes place within the IF(1) monolayer grown via S_1 , leading to thickening domains of IF(0) which will gradually develop into an ellipsoidal shape. Once the IF(0) domains touch the crystal growth front, they will induce the direct formation of IF(0). Therefore, S_1 , S_{10} , and S_0 can coexist at the same supercooling, which is unexpected.

EXPERIMENTAL SECTION

The LMW PEO fraction with chain end groups of $-OH$ (HPEO) at both ends, a number-average MW (M_n) of 3000 g/mol, and a polydispersity of 1.03 (denoted as HPEO3k below) was purchased from Polymer Laboratory. The static solution casting method for preparing the monolayer LMW PEO on mica surfaces has been described elsewhere.¹⁷ The isothermal crystallization processes were followed by *in situ* AFM (Nanoscope IIIA) coupled with a heat controller which was calibrated using standard materials to have an accuracy of ± 0.2 °C. Tapping mode was applied throughout this study using Veeco NanoProbe probes (model number, RTESP14; tip radius, ~ 8 nm; force, ~ 40 N/m; frequency, ~ 300 kHz). The height and phase images were recorded simultaneously at a scan rate of 1.5 Hz with a scan size of $7 \times 7 \mu\text{m}^2$ and a resolution of 256×256 , if not explicitly stated. The scan rate and resolution gave a typical time interval of 2.9 min between two neighboring images. The T_m of IF crystals were measured using a step-heating method described elsewhere^{17,20} and will be briefly mentioned in the Results.

Similar to that of other LMW PEO fractions, crystallization of HPEO3k ultrathin films on the mica surface with the pseudodewetted melt structure mainly leads to “flat-on” lamellar crystals. The basal surface normal of the flat-on crystal, which is usually parallel to the chain direction of PEO, is perpendicular to the substrate surface. The theoretical thickness of IF(n) crystals can be calculated as $l_u N / (n + 1)$, with $l_u = 0.278$ nm, the average length of one monomer in the crystalline lattice, and N , the degree of polymerization.²¹ For HPEO3k with $N = 68$, the theoretical thicknesses of IF(0), IF(1), and IF(2) crystals are thus 18.9, 9.5, and 6.3 nm, respectively. In experiments, the thicknesses of these three kinds of monolayer crystals can be unambiguously determined by analyzing the height images recorded by AFM. In most cases, the measured thicknesses agree very well with those theoretical thicknesses. In addition, the difference between the thicknesses of IF(0) and IF(1) crystals is so large that they can be easily visualized by the brightness of crystalline domains in the monochrome height image.

According to our experience, it is extremely difficult to isothermally grow PEO monolayer crystals from the pseudodewetted melt on hydrophilic substrates at a T_c above 30 °C. Therefore, a technique similar to the well-known self-seeding²² was adopted to overcome this difficulty.¹⁷ During the “self-seeding” procedure, the well-melted HPEO

monolayers were first quenched below 30 °C to induce a spontaneous crystallization. Afterward, the crystallized samples were slowly heated and annealed into IF(0) crystals. The temperature was further increased and carefully controlled to melt most IF(0) crystals. For the convenience of our experiments, the controlled melting was stopped when only a few small enough IF(0) crystals (their lateral size may be a few micrometers) were obtained. These small crystals embedded in the wetting layer or in dewetted melt droplets served as “seeds” to initiate the isothermal crystal growth. In our experiments, the typical “seed” density was about 1–2 per 100 μm^2 ; otherwise, the growth of neighboring crystals would correlate with each other because they would compete in consuming the surrounding melts. In the present study, both the IF(0) and IF(1) crystals were obtained using this technique. It was found that the apparent growth rates of IF(0) and IF(1) crystals were of the order of 1 nm/min, allowing us to use *in situ* AFM observation to trace the morphology evolutions with time.

RESULTS

Determination of $T_{\text{m}}(1)$ of the HPEO3k IF(1) Crystal. As mentioned previously, the area of interest is the phase selections of HPEO3k in the vicinity of $T_{\text{m}}(1)$. Therefore, identification of the location of $T_{\text{m}}(1)$ was the start point of our research. In bulk HPEO3k, the $T_{\text{m}}(0)$ of 57.6 °C can be reliably measured by differential scanning calorimetry (DSC). On the other hand, the IF(1) crystal was reported to be unstable under a heating rate slower than 4 °C/min, implying that the IF(1) of HPEO3k can rapidly relax to IF(0) upon a relatively slow heating process.²³ Nevertheless, during DSC heating scans with higher heating rates, the melting peak of IF(1) crystals emerged around 50.0 °C. However, this measured value of $T_{\text{m}}(1)$ is still way off the general trend of $T_{\text{m}}(1)$ for other PEO fractions obtained by Kovacs et al., which shows that the $T_{\text{m}}(1)$ of HPEO3k should be around 53.0 °C.

The $T_{\text{m}}(1)$ of the lamellae in the bulk state in fact only serves as a reference for where the $T_{\text{m}}(1)$ of monolayer IF(1) may locate. As one can expect, the monolayer crystals of LMW PEO on the mica surface should have their T_{m} values deviated from the bulk ones due to the change in surface free energy. We attempted to estimate the $T_{\text{m}}(0)$ and $T_{\text{m}}(1)$ of the monolayer HPEO3k crystals on the mica substrate using a step-heating method.¹⁷ In practice, HPEO melts were crystallized at a supercooling as small as possible to obtain a perfect crystalline monolayer with the desired fold number. Then, we slowly raised the temperature step by step with a typical interval of 0.1 °C. At each temperature, two successive AFM images were captured and compared. If shrinkage of crystal boundaries was identified between neighboring images, the annealing temperature at this step is considered to be just slightly higher than the T_{m} , and we take it as an apparent T_{m} (T_{m}^{a}). To obtain a T_{m}^{a} by a precise step-heating method, the procedure should be performed several times by a trial and error approach. For example, once the T_{m} is measured to be $T_{\text{m}1}^{\text{a}}$ after the sample was crystallized at $T_{\text{c}1}$, we will then repeat the step-heating procedure with a different T_{c} of $T_{\text{c}2}$ which is higher than $T_{\text{c}1}$ and thus is closer to $T_{\text{m}1}^{\text{a}}$. The corresponding $T_{\text{m}2}^{\text{a}}$ is expected to be higher than $T_{\text{m}1}^{\text{a}}$ because the defects within IF crystals are reduced as the supercooling is lowered. Repeating the above procedure several times will give a measured T_{m}^{a} of the monolayer IF crystals. Following this procedure, $T_{\text{m}}(0)$ and $T_{\text{m}}(1)$ of monolayer crystals of HPEO3k were measured to be close to 58.0 and 46.0 °C, respectively. We find that the step-heating method works very well for the

IF(0) monolayer, resulting in the AFM-measured $T_{\text{m}}(0)$ [i.e., the apparent $T_{\text{m}}(0)$] being comparable to that obtained in the bulk. However, the $T_{\text{m}}(1)$ of monolayer IF(1) of HPEO3k estimated is ~4 °C lower than that of bulk lamellae detected by DSC. The caution should be mentioned here is that IF(1) monolayers of HPEO3k have a strong tendency to thicken when the temperature approaches $T_{\text{m}}(1)$, which can also cause shrinkage of the lamellar size. As a result, the step-heating method we applied only gave an apparent $T_{\text{m}}(1)$ with an underestimation to some extent. Although both the $T_{\text{m}}(1)$ of the HPEO3k lamellae in the bulk state and the AFM-measured one of the monolayer do not truly reflect the thermodynamic stability of the IF(1) crystals, we consider that they are still valuable for guiding us to select a T_{c} -window for our experiments. As we will show below, when stepwise reducing the T_{c} , we in fact can catch a condition relevant to the zero-growth-rate of IF(1), which can lead to more precise determination of $T_{\text{m}}(1)$.

Various Phase Selection Pathways at Different T_{c} s. To clearly describe the phase selection behavior changes with T_{c} , we present the experimental results of isothermal crystallization of HPEO3k at various temperatures in a descending order. The simplest case of pathway selection occurs at T_{c} s above $T_{\text{m}}(1)$, wherein the crystallization of HPEO3k solely results in IF(0) lamellae, i.e., the pathway of S_0 is chosen. Figure 2 shows three typical height images recorded by AFM after crystallizing for a period of time at 56.0, 51.0, and 49.0 °C, respectively. The brighter domain near the center of the monolayer is the purposely saved “seed”. According to the series of AFM images sequentially recorded, we confirmed that only the IF(0) monolayer could be observed during the isothermal process. Therefore, the $T_{\text{m}}(1)$ of HPEO3k monolayer should be lower than 49 °C. When HPEO3k is crystallized at 56.0 °C, a temperature close to the $T_{\text{m}}(0)$, a faceted IF(0) single crystal is formed (see Figure 2a). It can be designated that the single crystals are bounded by two (100) and four (120) growth planes according the calculation performed by Shcherbina and Ungar.²⁴ This regular shape implies that the crystal growth in ultrathin film at such high temperature is nucleation-limited.¹⁷ By decreasing the T_{c} to 51.0 and 49.0 °C, the regular shape of IF(0) crystals directly grown from melt is more or less lost (see Figure 2, parts b and c). The growth planes remain straight when crystallized at 51.0 °C; however, they become unstable at 49.0 °C, implying that diffusion-limited growth may play a role. Obviously, disregarding whether the crystal growth follows nucleation- or diffusion-limited mechanism, only S_0 can be realized for all T_{c} s above 49.0 °C.

Isothermal crystallization of HPEO3k at 48.5 °C still followed the S_0 process, leading to the IF(0) lamellae directly. However, as T_{c} lowered to 48.0 °C, something more or less extraordinary was observed, as shown in Figure 3. It can be seen that the crystal perimeter continuously enlarges with time, most of which possesses a single thickness identical to that of IF(0), indicating that in this particular experiment the crystal growth mainly selects the pathway of S_0 . Nevertheless, in the meantime, we can observe a small protrusion of the monolayer with a thickness rather close to that of IF(1) (marked by the circles in Figure 3a–e). Intriguingly, the size of this protrusion neither grows nor contracts. Rather, the protrusion moves forward with the growth of the monolayer crystal during the whole period of experimental time. To illustrate clearly, we present in Figure 3f the section profile along the line indicated in Figure 3b, showing a two-step interface profile with the higher step corresponding

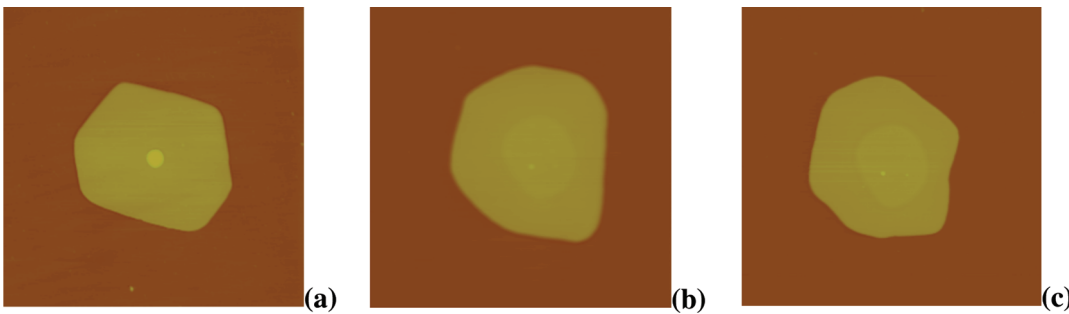


Figure 2. AFM height images for isothermal crystallization of HPEO3k at (a) 56.0 °C for 756.5 min, (b) 51.0 °C for 127.5 min, and (c) 49.0 °C for 89.4 min. The image size is 7 $\mu\text{m} \times 7 \mu\text{m}$ (a, b) and 9 $\mu\text{m} \times 9 \mu\text{m}$ (c), respectively.

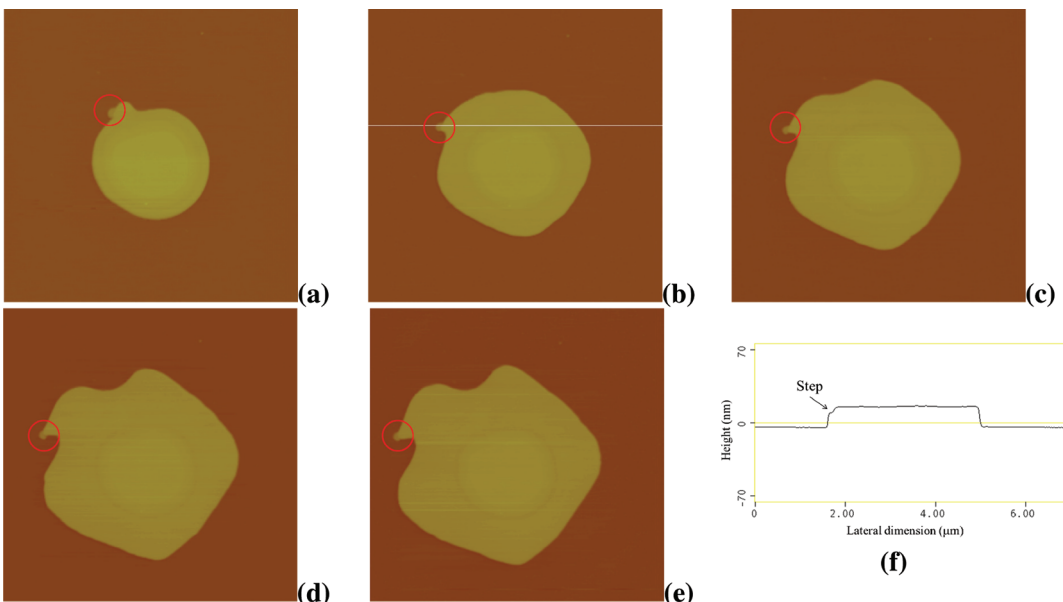


Figure 3. AFM height images for isothermal crystallization of HPEO at 48.0 °C for (a) 0.0 min, (b) 23.4 min, (c) 58.1 min, (d) 89.9 min, and (e) 104.4 min. The image sizes of a–e are 7 $\mu\text{m} \times 7 \mu\text{m}$.

to IF(0) and the lower one slightly larger than that of IF(1), inferring that the front end of the protrusion may be composed of chains with a nonintegral folding conformation. The protrusion with a two-step interface profile shown in Figure 3 in fact was detected frequently at the particular T_c of 48.0 °C. Sometimes, we even observed that the entire rim of the crystal growth front contained a thickness close to IF(1), which was immediately followed by IF(0). When we monitored the monolayer crystal growth of HPEO with M_n of 4250 g/mol, similar phenomenon was also observed when the T_c was set to be slightly lower than the $T_m(1)$ (unpublished data). This step-like interface profile can be taken as a signature of the composite nucleation, wherein the metastable protrusion or rim is sandwiched between the melt and the stable phase of IF(0). Therefore, the phase selection pathway belongs to S_2 . Figure 3 demonstrates that both S_0 and S_2 can coexist during HPEO3k crystallization at 48.0 °C.

When the crystallization of HPEO3k melt was carried out at a temperature below 48.0 °C but higher than 40.0 °C (around the melting temperature of IF(2) monolayer [$T_m(2)$]), the crystallization behavior became rather complicated, wherein the whole process could be divided into three stages. The typical result is shown in Figure 4 as a series of AFM images recorded at 47.0 °C.

The bright domain in Figure 4a is a monolayer crystal purposely saved as a “seed”. The “seed” possesses a thickness slightly larger than 19.0 nm, which may have occurred because the crystal that survived the “self-seeding” was composed of PEO chains with a relatively larger MW (note that HPEO3k still has a MW polydispersity). Interestingly, such a “seed” can only initiate the growth of the IF(1) crystals (Figure 4b). Therefore, at the first stage of crystallization, the transition pathway from melt to the IF(1) crystal, i.e., pathway of S_1 , is dominant. Furthermore, the existence of IF(1) indicates that the T_c of 47.0 °C should be lower than the $T_m(1)$ of HPEO3k monolayer. After the IF(1) crystal grew to some extent, the crystal growth enters the second stage, wherein the IF(0) crystals emerge out as nearly rounded, thickened domains distributed randomly inside the previously grown IF(1) monolayer. Figure 4c captures the birth of the first two IF(0) domains, and the later evolution of the growth pattern is shown in Figure 4d and 4e. Consequently, we observe another transition pathway of S_{10} , namely, from IF(1) to IF(0), coexisting with S_1 at the second stage of crystallization.

It is interesting to note that as the crystallization at 47.0 °C proceeded further, the IF(1) crystal would slow its growth, but the nucleation of thickening domains was not suppressed.

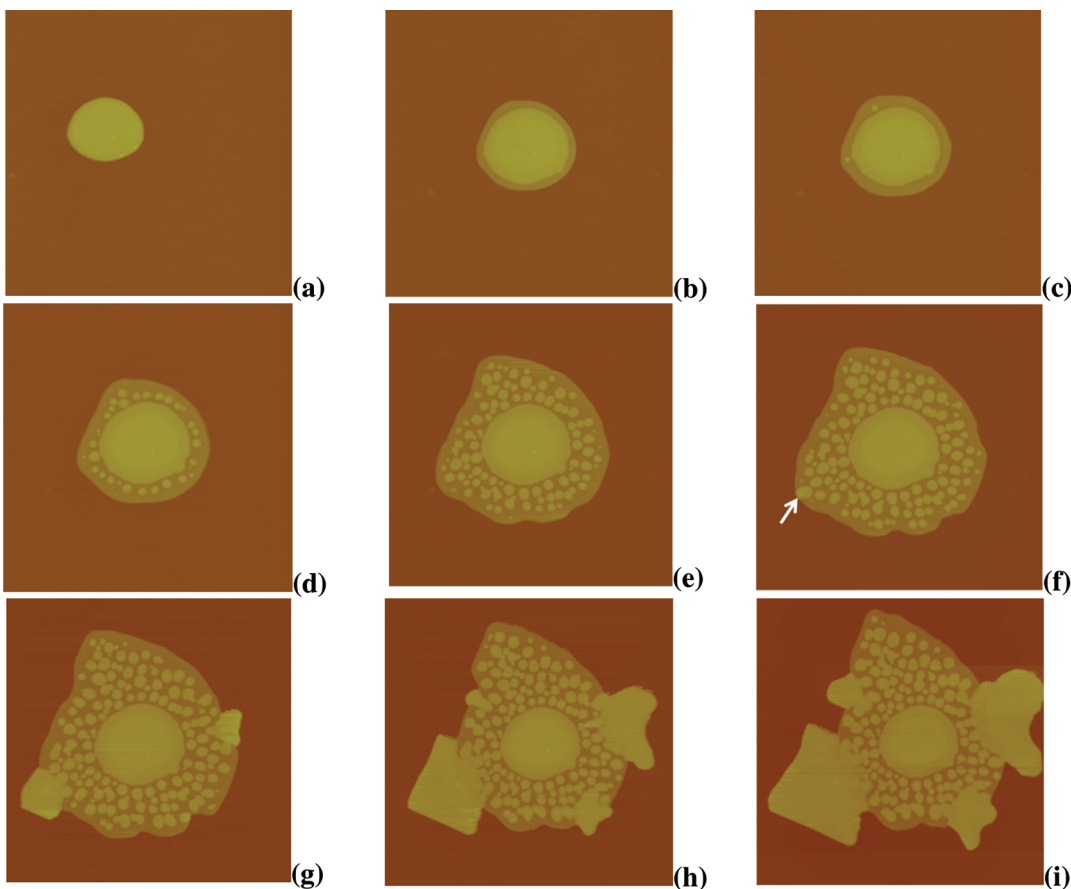


Figure 4. A set of AFM height images for isothermal crystallization of HPEO3k at 47.0 °C for (a) 0 min, (b) 11.8 min, (c) 17.6 min, (d) 29.2 min, (e) 58.0 min, (f) 69.7 min, (g) 87.0 min, (h) 121.2 min, and (i) 150.5 min. The image size is 7 μm × 7 μm (a-g) or 8 μm × 8 μm (h, i). The rounded bright region in the center of the crystal is the seed. The arrow in part f points to a thickening domain just protruding out of the IF(1) crystal boundary.

Therefore, there is a great opportunity for thickening domains to nucleate close enough to the growth front of the IF(1) crystal via the S_1 process. Figure 4f gives one such example of these special thickening domains, as indicated by the white arrow. It can be seen that a part of the lateral surface of the thickening domain is on the edge directly contacted with the melt. This exposure of the lateral surface of the thickening domain results in the third stage of HPEO3k isothermal crystallization at 47.0 °C, which induces the S_0 process of direct growth of IF(0) from the melt. As a result, at the third stage, we observe the three phase selection pathways of S_1 , S_{10} , and S_0 simultaneously. The newly grown IF(0) monolayer can be quite regular as shown by the bottom-left corners of Figures 4g–i. When looking more carefully at Figure 4h and Figure 4i, one can find that S_1 is suppressed significantly and will finally cease, and only the growth of IF(0) crystals will remain (see Discussion).

For the isothermal crystallizations performed at 47.5 °C or below 47.0 °C, the three stages could also be observed. In comparison to that of 47.0 °C, the lifetimes of the first and second stages were different, indicating that T_c mainly influenced the crystallization kinetics. Figure 5 depicts AFM images recorded at 47.5 °C, giving the snapshots typical for the different stages. The first stage is evident in Figure 5a. Compared to the observation at 47.0 °C, the second stage starts earlier but its lifetime is shorter, meaning that the S_{10} process is much faster. Many IF(0) domains, due to S_{10} , touch the growth front

sooner, resulting in the third stage of crystallization. As shown by Figure 5c–f, S_0 quickly becomes the main process to govern the crystallization at later times. In Figure 5f, all IF(1) crystals have been transformed to the IF(0) crystal. The IF(0) crystals formed via S_{10} are a bit thinner than the IF(0) crystals formed via S_0 , which can be seen from the slightly darker region around the seed in Figure 5f. This may be due to the fact that the S_{10} gives a less perfect IF(0) crystal containing a fraction of nonintegral folding chains. For T_c ranging from 40.0 to 46.0 °C, the lifetimes of the first and second stage were prolonged with lowering T_c , indicating that the pathway of S_{10} related to the IF(1) thickening became more and more difficult.

■ DISCUSSION

The AFM observations described above reveal that decreasing T_c results in more and more complex crystallization behavior of HPEO3k ultrathin film. We confirm that the melt crystallization of HPEO3k with the stable phase of IF(0) and the metastable phase of IF(1) possesses four possible phase selection pathways: S_0 and S_1 directly lead to IF(0) and IF(1), respectively; S_2 grows IF(0) crystals through a composite nucleation; the other pathway of S_{10} is transition of IF(1) → IF(0). Obviously, the pathway selection is highly supercooling dependent. Only S_0 is allowed above $T_m(1)$. The complexity appears when T_c is selected to be slightly lower than $T_m(1)$. As shown in Figures 4 and 5, the phase

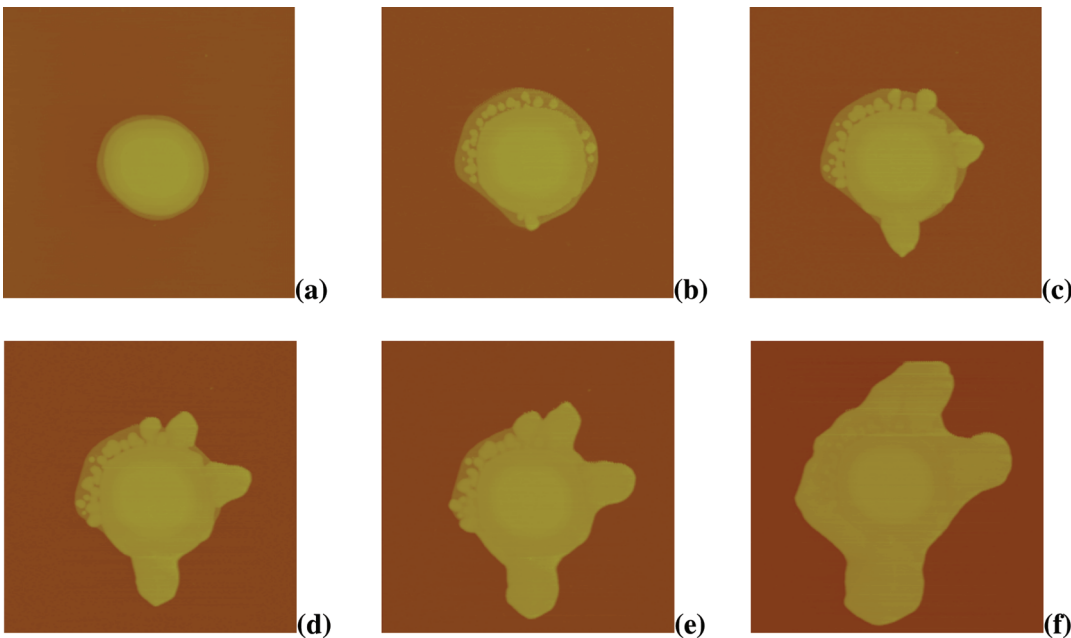


Figure 5. AFM height images for isothermal crystallization of HPEO at 47.5 °C for (a) 0 min, (b) 22.3 min, (c) 39.6 min, (d) 54.0 min, (e) 68.5 min, and (f) 111.8 min. The size of images is 7 $\mu\text{m} \times 7 \mu\text{m}$.

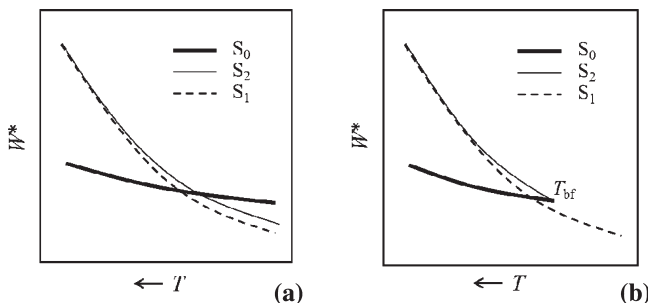


Figure 6. Nucleation barrier (W^*) as a function of temperature (T) predicted by (a) classical nucleation theory and (b) Gránásy–Oxtoby theory. The schematic drawings are based on the data in ref 19.

transition pathway is also time dependent, wherein the crystallization process can be divided into three stages. While at the first stage the crystallization solely belongs to S_1 , three different pathways of S_1 , S_{10} and S_0 can coexist at the third stage. We will discuss the supercooling and time dependence separately.

1. Supercooling Dependence of Phase Selection Pathways. In general, the supercooling dependence of phase transition pathways can be understood with the aid of the physical picture of nucleation theory. As shown in Figure 6a, the nucleation barriers based on CNT for pathways S_0 , S_1 , and S_2 all decrease with T_c . Despite the differences in nucleation barriers for these three phase selection pathways, they can happen simultaneously in principle below $T_m(1)$. However, if attention is given to the first stage of crystallization at 47.0 °C, we notice that only the IF(1) monolayer grows from the “seed”, suggesting that S_0 is largely forbidden. Recently, Gránásy and Oxtoby extended the CNT by considering a simplified triple-parabolic free energy.¹⁹ They conducted a detailed theoretical study based on Cahn–Hilliard theory and performed a full mapping of all possible phase selection pathways. Figure 6b schematically draws

a profile of the nucleation barriers as functions of temperature obtained by Gránásy and Oxtoby. In comparison with Figure 6a, there is a bifurcation point (T_{bf}) in Figure 6b where the nucleation barriers for the S_0 and S_2 processes become identical. Below the T_{bf} both profiles of S_0 and S_2 disappear, which means that only S_1 nuclei can be generated to initiate crystal growth. From this point of view, the T_{bf} of HPEO3k should be higher than 47.5 °C since at or below this temperature only the S_1 process is observed at the first stage of crystallization. The calculation of Gránásy and Oxtoby also suggests that the only pathway to form a stable phase below T_{bf} is via an uncorrelated solid-to-solid nucleation (i.e., S_{10} in our case) in the regions which have already crystallized into the metastable phase. In this context, although the Gránásy–Oxtoby theory was developed for primary nucleation, it can help to explain our experimental results obtained above 48 °C and also the behavior of the first and second stage of crystallization below 48 °C.

Identification of T_{bf} suggested by Gránásy–Oxtoby theory is one of the keys to understand the phase selection pathways in the HPEO3k ultrathin film crystallization. As mentioned, the T_{bf} should be higher than 47.5 °C. On the other hand, Figure 3 shows a step-like interface at $T_c = 48$ °C, of which the profile in Figure 3f resembles the “broad-interface” solution of Gránásy and Oxtoby’s results. It is predicted that the pathway S_2 can only exist between T_{bf} and the melting temperature of the metastable phase [here the $T_m(1)$].¹⁹ Moreover, the nucleation barriers of S_0 and S_2 become identical at T_{bf} (see Figure 5b). Accordingly, we can presume that the temperature of 48.0 °C lies in the range of $T_{bf} \sim T_m(1)$ for HPEO3k, and the location of T_{bf} should be 47.5 °C < $T_{bf} \leq 48$ °C.

When $T_c = 48.5$ °C, we only observed the direct growth of the IF(0) monolayer, a manifestation of pathway S_0 . This also suggests that the temperature of 48.5 °C crosses over the zero-growth condition of IF(1) crystals. In light of the above analysis, we can propose a more precise method for determining $T_m(1)$ of the monolayer IF(1) crystals on the basis of the AFM measured phase selection map. Compared with the aforementioned

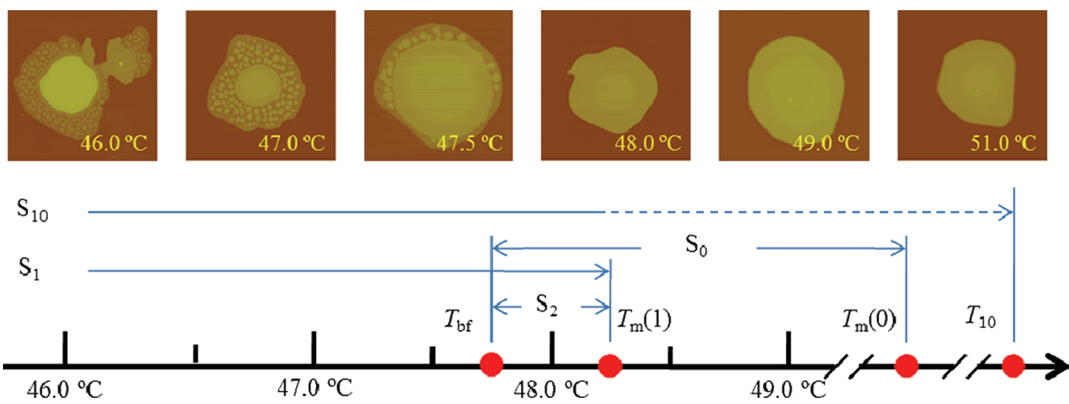


Figure 7. Possible phase selection pathways for crystallization of HPEO3k on mica surfaces. The AFM height images showing the typical morphologies of monolayer crystals isothermal crystallized at various temperatures are positioned in accordance with which temperature region they belong to. T_{bf} : bifurcation point; $T_m(1)$ and $T_m(0)$: melting temperatures of IF(1) and IF(0) crystals; T_{10} : the virtual temperature where IF(1) are in equilibrium with IF(0). Possible phase selection pathways are: melt \rightarrow IF(0) (S_0), melt \rightarrow IF(1) (S_1), IF(1) \rightarrow IF(0) (S_{10}), and the composite pathway built of the latter two (S_2). The temperature regions in which these phase selection pathways can exist are marked by the arrows. The dashed line in the right part of S_{10} arrow stands for an imaginary transition since it is impossible to grow IF(1) crystals above $T_m(1)$.

step-heating method, this method does not suffer from thickening, the specific morphology, and the defects within the crystal which may cause underestimation of the T_m . For HPEO3k, $T_m(1)$ of the monolayer shall be restricted to the range of 48.0 to 48.5 °C (see the bottom part of Figure 7). This gives an estimate of $T_m(1)$ as 48.3 °C with an error less than 0.3 °C, of which the value is significantly larger than that measured by the step-heating method (~ 46.0 °C). With the estimation of T_{bf} and $T_m(1)$, Figure 7 depicts our phenomenological mapping between available phase selection pathways observed in our experiments and that predicted by the Gránásy–Oxtoby theory, wherein only the first and second stage of crystallization below 48.0 °C are taken into account. In the same figure, typical morphologies of HPEO monolayer crystals crystallized at 46.0, 47.0, 47.5, 48.0, 49.0, and 51.0 °C are presented.

2. Crystallization Time Dependence of the Phase Selection Pathways. While the Gránásy–Oxtoby theory can be phenomenologically applied to explain many of our experimental observations, the puzzle remains: why is S_0 forbidden at the initial stage, yet S_0 and S_1 can coexist at the last stage of crystallization at below 48.0 °C, showing that the pathway selection is further dependent on crystallization time? This observation is also incompatible with the surface nucleation theory of polymer crystallization, which assumes that one thickness corresponding to the maximum crystal growth rate should be selected at a fixed supercooling. As fold length fluctuation is allowed at the crystal growth front, one may argue that another thickness with a slightly smaller growth rate can also have a chance to grow. However, considering that the thickness of IF(0) is twice that of IF(1), the thickness difference shall be beyond the fluctuation range. It has been reported that the bulk crystallization of low MW PEO fractions can form nonintegral folded chain (NIF) crystals prior to IF crystals.^{25,26} The fold length of NIF crystals is inversely proportional to the supercooling, which agrees with the prediction of surface nucleation theory. Through lamellar thickening or thinning, the NIF crystals transfer into IF crystals. However, we could not detect monolayer NIF crystals of HPEO3k during the S_0 or S_1 process, which may be due to the possibility that NIF crystals existed at the growth front just with a very short lifetime or very small width.

2.1. The S_{10} Process. As shown in Figures 4 and 5, the S_0 process in the third stage is closely related to the prior S_{10} stage. That is, only after some IF(0) domains via the S_{10} process touch the growth front will they trigger the S_0 process. Here, we should make a few comments on the S_{10} process first. When entering the second stage of crystal growth, the thickened domains of IF(0) first appear with a rounded shape. The growth pattern of IF(0) domains is quite similar to the thickening of the IF(1) monolayer of the LMW PEO fraction with M_n of 2000 g/mol (HPEO2k) previously studied.²⁷ Also using *in situ* AFM, we monitored the morphology evolution of IF(1) monolayers of HPEO2k annealed at various temperatures below its $T_m(1)$. On the basis of both experimental observation and phase field simulation, we consider that after complete crystallization, the thickening is a solid-to-solid transition from IF(1) crystals to IF(0) crystals following a nucleation and growth mechanism. While the longitudinal sliding motion of chains within the crystalline lattice provides the manner of thickening, the surface free energy dominates the nucleation barrier. Here, the initiation of S_{10} can be understood based on our previous result. When the crystallization temperature is close to $T_m(1)$, the fold surface free energy is lower compared with that at lower temperatures, leading to the thickening being much easier. As a result, S_{10} can occur accompanied by the continuous growth of mother phase of IF(1) (the S_1 process). Moreover, the lifetimes of the first and second stage increase with lowering T_c . By quenching the HPEO3k melt to a temperature close to $T_m(2)$ (~ 40.0 °C), S_{10} was only observed when IF(1) crystals grew to a much larger size than those in the cases of 46.0–47.5 °C.

During the growth of the thickening domains via S_{10} , we observed that the initial round shape would change to be more or less elongated. As illustrated in Figure 8 of an AFM image recorded at 47 °C, the contour of the thickening domains can be fitted into an ellipse, most of whose long axes point to the growth front of the IF(1) monolayer. The oriented growth of IF(0) thickening domains through S_{10} has been neither predicted by theory nor observed by previous experiments. The cause of this orientation is not very clear. Here, we just give possible explanations. It is suggested that the newly attached molecular chains on the crystal growth front are far from equilibrium.²⁸ The

folds on the top surface are usually loose, the cilia are much longer and the length of stems that are already fitted in the crystalline lattice is shorter in comparison with that in the final state. Therefore, we can imagine that polymer chains within the area close to the growth front must be most mobile, which can undergo chain-unfolding much easier. Consequently, the growth of thickening domains will proceed more along the normal of the crystal growth front than other directions.

On the other hand, the chain-unfolding certainly creates lattice vacancies which need to be filled. According to our previous observation, thickening of the IF(1) monolayer of HPEO2k after complete crystallization can result in the shrinkage of the lateral size of monolayer crystals.²⁷ This implies that the adjacent chains can “jump” into the vacancies, resulting in vacancy diffusion to the perimeter of the lamella. This process may also take place in the case of simultaneous S_1 and S_{10} processes. Meanwhile, the other way to fill the vacancies is the “reeling in” of chains from the surrounding melt.^{13,29} Recently, a dynamic Monte Carlo simulation by Ma et al. showed that the lamellae of short-chain

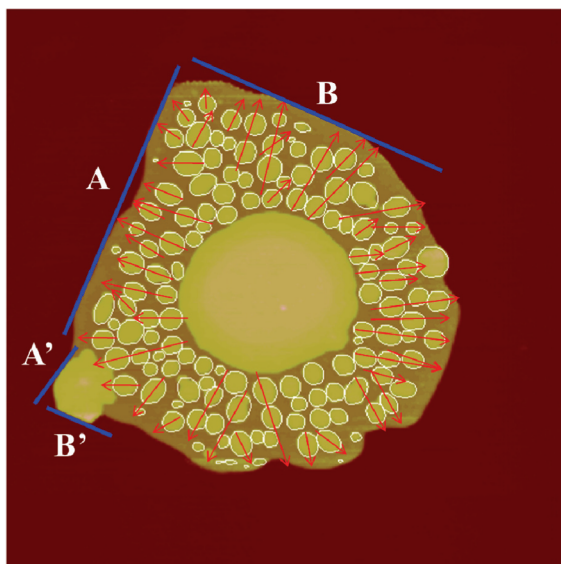


Figure 8. Directed growth of thickening domains via S_{10} at 47.0 °C. Red arrows are drawn to guide eyes along the direction of long axes of the fitted ellipses. The straight lines, A, B and A', B', denote the growth fronts of IF(1) crystal and IF(0) crystal, respectively.

polymers grown at a temperature lower than $T_m(1)$ possess a growth front dominated by IF(1) chains, and the chain-extension that leads to the IF(0) lags behind the growth front.³⁰ The simulation demonstrates that during thickening, numerous molten chains are sucked into the lamella through the basal planes. For the case studied here, we presume that to fill the voids due to chain-unfolding the materials can come from the wetting layer on the mica surface. The molten molecules may climb up the top surface of the crystalline monolayer and then diffuse to the voids. This directional material transportation can also be a reason to account for the oriented growth of the IF(0) domains within the IF(1) mother phase which is growing forward in the meantime.

2.2. Competitions between S_{10} and S_1 and between S_0 and S_1 . The growth of thickening domains inside the monolayer (S_{10}) competes with the growth of IF(1) mother phase (S_1). We measured the volumes of the IF(0) and IF(1) [denoted as $V(0)$ and $V(1)$, respectively] as functions of the crystallization time after the system entered the second stage at 47.0 °C (see Figure 9a). It is intriguing to note that $V(0)$ increases much faster than $V(1)$. While the volume increase of IF(1) only gains at the crystal growth front, more and more nucleation events of IF(0) domains occur which accelerate the transformation from IF(1) to IF(0). As shown in Figure 9a, $V(0)$ crosses over $V(1)$ at about 40 min. The fast S_{10} process can eventually lead to some IF(0) domains touching the melt-crystalline interface, signaling the onset of the third stage which is at 69.7 min (indicated by the dashed line in Figure 9a).

We further observe that the increase of $V(1)$ levels off after 78.4 min, and afterward, the S_{10} and S_0 become dominant. This crystallization behavior can be further demonstrated by the propagation of the lateral dimensions of the HPEO3k monolayer. We plot in Figure 9b the distances (d) between the approximately straight growth fronts and the “seed” center as a function of time. The growth fronts concerned here are indicated by the solid lines in Figure 8, denoted by A and B for the IF(1) fronts and A' and B' for the IF(0) fronts, respectively. In Figure 9b, the initial d of all of these growth fronts is shifted to 0. Apparently, the growth fronts of A and B move forward linearly at first; the later deviation from linearity with the onset at around 75 min is most probably caused by the later on apparent direct growth of IF(0). Moreover, for the nearly parallel fronts of A and A' at the same side of the monolayer, the growths of A' (S_0) and of A (S_1) compete with each other. It seems that the growth of A' can suppress and eventually stop the growth of A. On the other

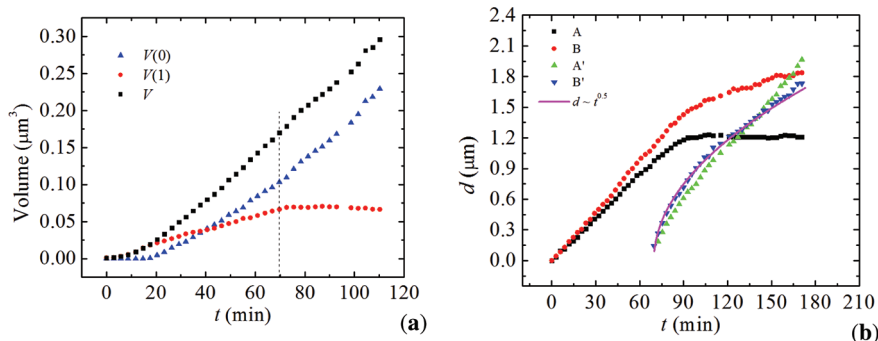


Figure 9. (a) Volumes of IF(1) crystal [$V(1)$] and IF(0) crystal [$V(0)$] and their sum V as functions of crystallization time at 47.0 °C. (b) Distance (d) between the approximately straight growth front and a reference point (the center of the seed is chosen) increases with crystallization time for IF(1) crystals and IF(0) crystals at 47.0 °C. A, B and A', B' denote four selected growth fronts, which are marked in Figure 8. The initial distances of these four growth fronts are shifted to 0 and their following distances are shifted accordingly.

hand, the growths of A' and B' have little impact on the growth of B at the other side of the monolayer. This indicates that the interference between the S₁ and S₀ process also depends on where the two events happen. If the S₁₀ process could result in exposing many IF(0) domains to the melt all around the IF(1) growth front, as shown in Figure 5 of HPEO3k crystallized at 47.5 °C, the S₁ process could be completely stopped sooner.

2.3. Possible Explanation of S₀ Occurring below T_{bf}. Why the “seeds” cannot initiate S₀ at the beginning of crystallization but the thickened domains at the late stage can is not fully understood at present. We presume that it may be related to the crystallization mechanism switching from nucleation-limited to diffusion-limited. Considering the system with the “seed” contacting the PEO wetting layer on the mica surface, the molten molecules are abundant at the interface initially. Crystallization certainly consumes the melt at the growth front, creating a depletion zone when the molten molecules are reluctant to diffuse toward the lamellar growth front. As a result, the wetting layer in the depletion zone may not be fully covered by the PEO molecules but with the molecules distributing discretely on the substrate, which can be described using a model of “two-dimensional (2D) solution”.¹⁷ Therefore, the diffusion field can be characterized by the molecular concentration varying with distance: the molecular concentration is lowest at the crystal front and gradually approaches the value of the wetting layer at the end of depletion zone.

For the HPEO3k ultrathin film crystallization studied, we consider that at the very beginning, the crystallization shall be nucleation-limited. Right after quenching to a desired T_c, the “seed” is surrounded by the wetting layer which can supply sufficient molten molecules ready for crystallization. In this case, the height of the nucleation barrier determines the phase selection pathway, as predicated by the Gránásy-Oxtoby theory. Although the IF(1) crystal only gained a shallow thermodynamic stability at a temperature slightly lower than T_m(1), it can exist as a component of the composite nucleation (S₂) and even be the sole choice at T_c lower than T_{bf} (S₁).

As the isothermal crystallization proceeds to a certain extent, the depletion zone forms. At a fixed T_c the nucleation barrier is not altered, but the slow diffusion of molten molecules toward the crystal front can become the rate-determining step, leading to a diffusion-limited process. In Figure 9a, the total crystal volume V = V(1) + V(0) is also plotted, which increases approximately linearly with time (t) after the first stage, i.e., V ∝ t. Moreover, for the growth of the A' and B' fronts shown in Figure 8, we find that the behavior of d versus t fairly follows d ∝ t^{0.5} (see the solid line in Figure 9b). These time dependences imply that the growth of crystals at the later stage is largely diffusion-limited.¹⁷ Therefore, we imagine that at the melt-crystalline interface, the molten molecules are not crowded, and they have sufficient time to adjust their conformation to a state with lower free energy. Direct deposition of an IF(0) layer on the IF(1) front is still very difficult due to the penalty of surface free energy. However, the growth of IF(0) crystals directly from the melt can be initiated at the interface of the exposed IF(0) domains created via S₁₀. In addition, as shown in Figure 8, the IF(0) domains are ellipsoidal with a curvature much larger than that of the IF(1) front. The larger curvature will result in larger growth rate as long as the crystal growth is diffusion-limited. As a result, the later S₀ process depletes the surrounding materials significantly and eventually suppresses the S₁ process.

The explanation mentioned above actually invokes the physical picture of “self-poisoning”. We are aware that Ungar and co-workers

have reported a similar phenomenon when they crystallized n-C₁₉₈H₃₉₈ in 1-phenyldecano solution at T_c = 97.4 °C.³¹ In their experiments, pseudohexagonal plate-like folded-chain crystals were formed at the initial stage. The metastable equilibrium between folded-chain crystals and pseudosaturated solution was established shortly thereafter. After some time, the platelet crystals were suddenly replaced by highly elongated IF(0) crystals. The transformation from folded-chain crystals to IF(0) crystals is assumed to be triggered by some randomly formed IF(0) crystals. It is suggested that at high concentrations, the growth of IF(0) crystals is highly suppressed by the “wrong” but nearly stable chain-folded deposition which “pins down” the underlying molecules at the growth front and hinders their extension; chain extension is only possible after the overlayer is removed. In this case, “self-poisoning” plays a great role in controlling the crystallization behavior. The growth of IF(0) crystals depletes the surrounding solution which in turn induces the growth of other IF(0) crystals in the vicinity, as the suppressing effect of high concentration releases. As our pseudodewetted melt crystallization can be mapped onto a “2D solution” crystallization,^{17,32} the “self-poisoning” mechanism emphasized by Ungar et al. shall also be helpful for understanding the S₀ process occurring at the third stage of crystallization at T_cs below T_{bf}. Similar to the case of solution crystallization of n-C₁₉₈H₃₉₈, the decreasing of molecular concentration further enhances the growth of IF(0) crystals. Therefore, the pathway of S₀ once invoked will sustain and dominate the later crystal development.

CONCLUSION

In summary, four phase selection pathways, namely, melt → IF(0) (S₀), melt → IF(1) (S₁), IF(1) → IF(0) (S₁₀), and the composite pathway (S₂) have been revealed in this work when HPEO3k crystallizes from the pseudodewetting melt at temperatures near T_m(1). Whether these pathways occur alone or together depend on the supercooling. Below T_{bf} crystallization time also becomes an important factor, which may be related to transportation and supply of molten molecules. Instead of relying on the kinetic theory, we treat the current system as a realization of the three-phase model. The phase selection behavior of the three-phase model can be described by a modified classical nucleation theory—the Gránásy–Oxtoby theory. By carefully examining the change of morphology at different T_cs, we can successfully assign all phase selection pathways to suitable temperature regions according to the Gránásy–Oxtoby theory. As a unique example of the three-phase model which can be visualized *in situ* and in real space, it gives us much more opportunities to study its phase transition behavior at different supercoolings. More generally, our result gives an example to the Ostwald’s stage rule, which suggests that a phase transformation from an unstable state to the stable state would first form a less stable state, i.e., the so-called metastable state if it exists, and then pass sequential metastable states with increasing stability.

In this study, we also discussed a preliminary yet surprising finding which concerns the preference of growth direction of thickening domains and the coexistence of S₁, S₁₀, and S₀ at the late stage of crystallization at T_c below T_{bf}. These two phenomena observed are beyond expectation, raising questions for further study. Tentatively, we suggest that they may be related to the material transportation and crystallization mechanism switching from nucleation-limited to diffusion-limited, respectively. Quantitative studies on kinetics of all phase selection

pathways, especially of the pathway S₁₀ will be reported in the near future. Moreover, we suggest that the computer simulation techniques, such as that based on the phase field theory which has been proven to be a powerful tool for studying thickening of annealed monolayer crystals, should also give some new insight into the phase selection pathways and morphological transformations in LMW polymers during crystallization.

■ AUTHOR INFORMATION

Corresponding Author

*E-mail: eqchen@pku.edu.cn (E.-Q.C.).

Present Addresses

[†]Key Laboratory of Molecular Engineering of Polymers of Ministry of Education, Department of Macromolecular Science, Fudan University, Shanghai 200433, China

■ ACKNOWLEDGMENT

The authors appreciate the discussions with Prof. S. Z. D. Cheng. This work was supported by the National Nature Science Foundation of China (NNSFC Grants: 20774006, 20990232, 21074003, and 21004033). Y.-X.L. also acknowledges the support of the Shanghai Postdoctoral Scientific Program (2011). We are grateful to Dr. Ryan Van Horn for correcting of our English writing.

■ REFERENCES

- (1) Cheng, S. Z. *Phase Transitions in Polymers: The Role of Metastable States*; Elsevier: Amsterdam, 2008.
- (2) Keller, A.; Goldbeck-Wood, G. Polymer Crystallization: Fundamentals of Structure and Crystal Growth of Flexible Chains. In *Comprehensive Polymer Science: 2nd Supplement*, Aggarwal, S. L., Russo, S., Eds.; Elsevier: Oxford, U.K., 1996; pp 241.
- (3) Reiter, G.; Sommer, J. U. *Polymer Crystallization: Observations, Concepts and Interpretations*; Springer-Verlag: Berlin and Heidelberg, Germany, 2003.
- (4) Reiter, G.; Strobl, G. R. *Progress in Understanding of Polymer Crystallization*; Springer: Berlin and Heidelberg, Germany, 2007.
- (5) Hoffman, J. D. *Macromolecules* **1986**, *19*, 1124.
- (6) Ungar, G.; Keller, A. *Polymer* **1987**, *28*, 1899.
- (7) Organ, S. J.; Ungar, G.; Keller, A. *Macromolecules* **1989**, *22*, 1995.
- (8) Boda, E.; Ungar, G.; Brooke, G. M.; Burnett, S.; Mohammed, S.; Proctor, D.; Whiting, M. C. *Macromolecules* **1997**, *30*, 4674.
- (9) Ungar, G.; Putra, E. G. R.; de Silva, D. S. M.; Shcherbina, M. A.; Waddon, A. J. *Adv. Polym. Sci.* **2005**, *180*, 45.
- (10) Sadler, D. M.; Gilmer, G. H. *Phys. Rev. Lett.* **1986**, *56*, 2708.
- (11) Sadler, D. M.; Gilmer, G. H. *Phys. Rev. B* **1988**, *38*, 5684.
- (12) Higgs, P. G.; Ungar, G. *J. Chem. Phys.* **1994**, *100*, 640.
- (13) Kovacs, A. J.; Gonther, A.; Straupe, C. J. *Polym. Sci. Polym. Symp.* **1975**, *50*, 283.
- (14) Cheng, S. Z. D.; Chen, J. H. *J. Polym. Sci., Part B: Polym. Phys.* **1991**, *29*, 311.
- (15) Reiter, G.; Sommer, J. U. *Phys. Rev. Lett.* **1998**, *80*, 3771.
- (16) Israelachvili, J. N. *Intermolecular and Surface Forces*; 2nd ed.; Academic Press Limited: London, 1991.
- (17) Zhu, D. S.; Liu, Y. X.; Chen, E. Q.; Li, M.; Chen, C.; Sun, Y. H.; Shi, A. C.; VanHorn, R. M.; Cheng, S. Z. D. *Macromolecules* **2007**, *40*, 1570.
- (18) Zhu, D. S.; Liu, Y. X.; Chen, E. Q.; Li, M.; Cheng, S. Z. *Acta Polym. Sin.* **2006**, *1125*.
- (19) Gránásy, L.; Oxtoby, D. W. *J. Chem. Phys.* **2000**, *112*, 2410.
- (20) Zhu, D. S.; Liu, Y. X.; Shi, A. C.; Chen, E. Q. *Polymer* **2006**, *47*, 5239.
- (21) Takahashi, Y.; Tadokoro, H. *Macromolecules* **1973**, *6*, 672.
- (22) Kovacs, A. J.; Gonther, A. *Colloid Polym. Sci.* **1972**, *250*, 530.
- (23) Buckley, C. P.; Kovacs, A. J. *Colloid Polym. Sci.* **1976**, *254*, 695.
- (24) Shcherbina, M. A.; Ungar, G. *Macromolecules* **2007**, *40*, 402.
- (25) Cheng, S. Z. D.; Zhang, A.; Barley, J. S.; Chen, J.; Habenschuss, A.; Zschack, P. R. *Macromolecules* **1991**, *24*, 3937.
- (26) Cheng, S. Z. D.; Zhang, A.; Chen, J.; Heberer, D. P. *J. Polym. Sci., Part B: Polym. Phys.* **1991**, *29*, 287.
- (27) Liu, Y. X.; Li, J. F.; Zhu, D. S.; Chen, E. Q.; Zhang, H. D. *Macromolecules* **2009**, *42*, 2886.
- (28) Hoffman, J. D. *Polymer* **1991**, *32*, 2828.
- (29) Point, J. J.; Kovacs, A. J. *Macromolecules* **1980**, *13*, 399.
- (30) Ma, Y.; Qi, B.; Ren, Y.; Ungar, G.; Hobbs, J. K.; Hu, W. *J. Phys. Chem. B* **2009**, *113*, 13485.
- (31) Ungar, G.; Mandal, P. K.; Higgs, P. G.; de Silva, D. S. M.; Boda, E.; Chen, C. M. *Phys. Rev. Lett.* **2000**, *85*, 4397.
- (32) Liu, Y. X.; Chen, E. Q. *Coord. Chem. Rev.* **2010**, *254*, 1011.